

Integral resonant control of collocated smart structures

Sumeet S Aphale, Andrew J Fleming and S O Reza Moheimani¹

School of Electrical Engineering and Computer Science, The University of Newcastle, Australia

E-mail: reza.moheimani@newcastle.edu.au

Received 13 July 2006, in final form 3 January 2007

Published 9 February 2007

Online at stacks.iop.org/SMS/16/439

Abstract

This paper introduces integral resonant control, IRC, a simple, robust and well-performing technique for vibration control in smart structures with collocated sensors and actuators. By adding a direct feed-through to a collocated system, the transfer function can be modified from containing resonant poles followed by interlaced zeros, to zeros followed by interlaced poles. It is shown that this modification permits the direct application of integral feedback and results in good performance and stability margins. By slightly increasing the controller complexity from first to second order, low-frequency gain can be curtailed, alleviating problems due to unnecessarily high controller gain below the first mode. Experimental application to a piezoelectric laminate cantilever beam demonstrates up to 24 dB modal amplitude reduction over the first eight modes.

1. Introduction

In many industrial, scientific and defence applications, the presence of noise and vibration is of significant concern; see for example [1–3]. The field of smart structures, or structures with integrated sensors and actuators, has arisen to offer improved vibration control in applications where passive techniques are either insufficient or impractical.

The two significant design tasks in active structural control are the selection and integration of actuators and sensors, and the control system design. In this work a new control methodology is introduced for the most common class of smart structures: those with integrated piezoelectric actuators and sensors. Due to their small volume, low weight and ease of structural integration, piezoelectric sensors and actuators have been the overwhelming transducer of choice for smart structures; see [4–7] for an introduction to the use of piezoelectric transducers in structural actuation and sensing.

It is well known that there are a number of difficulties associated with the control of flexible structures, the foremost of which are: variable resonance frequencies; high system order; and highly resonant dynamics. Traditional control system design techniques such as LQG, H_2 and H_∞ commonly appear in research works and have been well documented; see

for example [8–11]. Unfortunately, the direct application of such techniques has the tendency to produce control systems of high order and possibly poor stability margins.

Controllers based on the underlying structure of a collocated resonant mechanical system have proven to offer greater robustness, performance, and ease of implementation relative to traditional techniques. The most useful characteristic of a collocated system is the interlacing of poles and zeros up the $j\omega$ axis. This results in a phase response that lies continuously between 0° and -180° . Positive position feedback (PPF) [12] is a popular technique exploiting this property. PPF controllers are stable in the presence of uncontrolled in-bandwidth modes, and roll off quickly at higher frequencies, reducing the risk of destabilizing systems with high-frequency dynamics. However, PPF controllers are also equal in order to the system that they are designed to control, require a model-based design process (often requiring a nonlinear search), and are difficult to tune if more than one mode is to be controlled. Velocity feedback [13] is another technique that exploits the known phase response of collocated systems. In theory, velocity feedback implements pure viscous damping with a phase margin of 90° . Unfortunately, the high-frequency gain must be attenuated to avoid noise amplification and destabilization due to unmodelled or non-collocated dynamics. Although velocity feedback has been applied in practice, it generally results in relatively low performance and

¹ Author to whom any correspondence should be addressed.

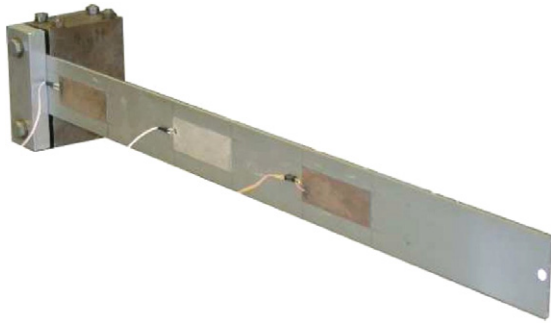


Figure 1. Picture of the cantilever beam.
(This figure is in colour only in the electronic version)

poor phase margin (due to the two additional poles required at high frequencies). Resonant control is another approach that has been applied successfully to collocated resonant systems [14]. A resonant controller guarantees closed-loop stability in the presence of uncontrolled out-of-band modes of the structure. The high-pass nature of the controller, however, may not be suitable in certain applications.

The control design in this work is based on augmenting the feed-through of a collocated system; that is, to add a small portion of the actuator signal to the sensor signal. It is shown in section 3 that this procedure results in the addition of a pair of resonant system zeros at an arbitrary frequency. Choosing this frequency lower than the first mode results in a compound system with interlaced zeros then poles, rather than poles then zeros. The phase response of this system lies between 0° and -180° . This property can be exploited through the use of direct integral feedback, which results in a loop phase response that lies between -90° and $+90^\circ$, i.e. has a phase margin of 90° and infinite gain margin. Integral resonant control, IRC, has the benefit of substantial damping augmentation while naturally rolling off at higher frequencies.

The objectives and scope of this work together with a description of the experimental apparatus are contained in the following section. The characteristics of collocated systems, feed-through augmentation, and IRC design are then discussed in section 3. Experimental results demonstrating up to 24 dB reduction over eight modes and conclusions follow in sections 4 and 5.

2. Objectives

The main objective of this work is to damp the low-frequency modes of a collocated resonant mechanical system exhibiting interlaced poles and zeros. The interesting properties of such transfer functions will be described and analysed. A mathematical proof for the pole-zero interlacing phenomenon in such transfer functions will be given. It will be shown that by adding a specific feed-through term to this transfer function, the implementation of simple second-order controllers that damp vibrations over multiple low-frequency resonant modes is possible. The appropriate feed-through term is identified and a parametric equation will be provided for the same. A cantilever beam, which is clamped at one end and free at the other end, is a well-known example of a resonant mechanical

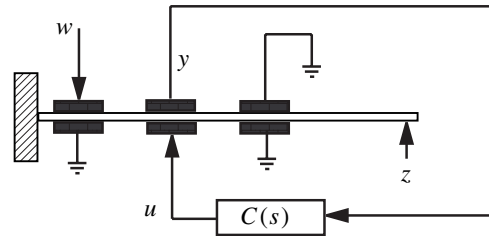


Figure 2. Schematic diagram of the control strategy showing the inputs and outputs.

system. It is susceptible to high amplitude vibrations when disturbed and will be used to validate experimentally the theories presented in this work.

2.1. Experimental setup

Figure 1 shows the experimental setup used in this work. The cantilever beam has three pairs of collocated piezoelectric patches attached to it. For this work, one collocated pair is used for actuation and sensing. The second collocated pair is shorted, thus for all practical purposes it has no effect on the open- or closed-loop beam dynamics. Of the third collocated pair, one patch is shorted and the other is used as an independent disturbance source.

The cantilever beam is treated as a two-input two-output system; see figure 2. The inputs are the control voltages applied to the collocated actuator patch (u) and the disturbance generated by the third (non-collocated) piezo-patch (w). The outputs are the collocated sensor voltage (y) and the tip displacement (z).

The frequency response function (FRF) $G_{ij}(j\omega)$ is a 2×2 matrix where each element $G_{ij}(j\omega)$, $i, j = 1$ and 2 , corresponds to a particular combination of the input and output (for example, $G_{yw}(j\omega) = y(j\omega)/w(j\omega)$ when $u = 0$). These FRFs are determined by applying a sinusoidal chirp (from 5 to 250 Hz) as inputs (w and u) to the corresponding piezoelectric actuators and measuring the output signals (y and z). The chosen frequency range captures the first three resonant modes of the cantilever beam. All frequency response data was measured using a Polytec scanning laser vibrometer (PSV-300).

3. Controller design

For the purpose of control design and analysis, a model of the system is required. A subspace based modelling technique [15] is used to procure an accurate model of the experimental system. Figures 3 and 4 show the magnitude and phase responses of the model and experimental system. The model captures the dynamics of the system with sufficient accuracy.

3.1. Properties of collocated transfer functions

The transfer function associated with a single collocated actuator/sensor pair displays many interesting properties [16, 17], one of which is that the poles and zeros of the system interlace. This ensures that the phase of a collocated transfer function will be between 0° and -180° . The system transfer function

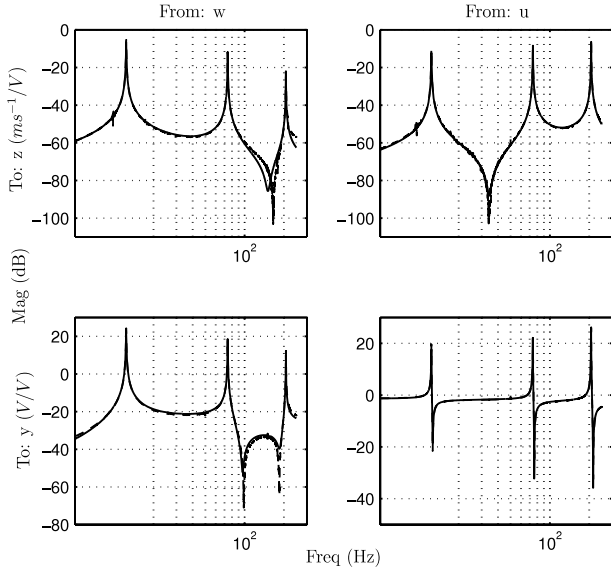


Figure 3. Magnitude response in dB of the measured (---) and modelled (—) system.

can be represented as the sum of many second-order blocks and can be written as

$$G(s) = \sum_{i=1}^M \frac{\alpha_i}{s^2 + 2\zeta_i\omega_i s + \omega_i^2} \quad (1)$$

where $\alpha_i > 0 \quad \forall i$ and $M \rightarrow \infty$ [18]. For all practical applications a very large but finite M represents the number of modes that sufficiently describe the elastic properties of the structure under excitation. In most scenarios, control of only a limited bandwidth is of importance. Typically, $N < M$ modes of the structure would fit within this bandwidth, while modes $N + 1$ and above are left uncontrolled. It is common practice to truncate the model of the system to include only those modes which are to be controlled. This truncation introduces significant errors, as the in-bandwidth zeros of the system are highly dependent on the out-of-bandwidth poles. Hence, when the model is truncated, the in-bandwidth zero dynamics are significantly perturbed. To account for this zero perturbation, a feed-through term is added. It has been shown that a constant feed-through is sufficient to model the effect of high-frequency modes on low-frequency zeros [19]. The truncated model can be written as

$$\tilde{G}(s) = \sum_{i=1}^N \frac{\alpha_i}{s^2 + 2\zeta_i\omega_i s + \omega_i^2} + D \quad (2)$$

such that $D \in \mathbb{R}$. Note that the collocated beam transfer function $G_{yu}(s)$ is of the form (2).

3.2. The effect of feed-through on pole-zero interlacing

The results in this section will explain the interlacing pole-zero pattern exhibited by the collocated transfer function $G_{yu}(s)$. The effect of a particular choice of feed-through, D , will also be explained. Zero damping is assumed for the sake of brevity, however the results can easily be extended to systems with

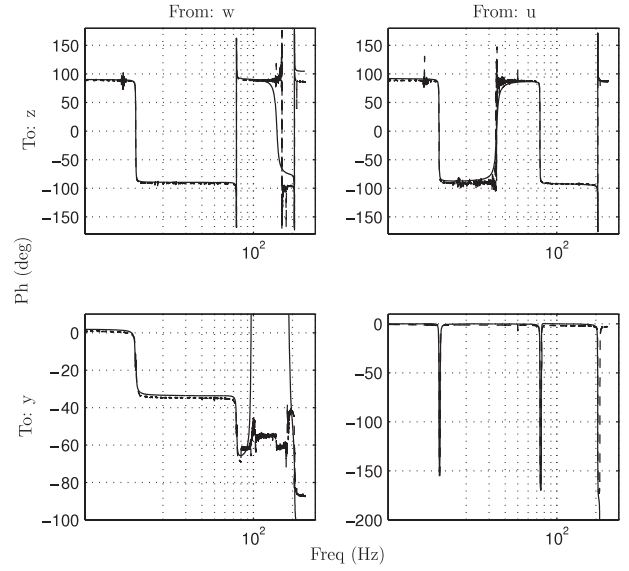


Figure 4. Phase response of the measured (---) and modelled (—) system.

damping. The following theorem shows that a system obtained by adding N second-order sections of the form $\frac{\alpha_i}{s^2 + \omega_i^2}$ has N pairs or complex conjugate poles and $N - 1$ pairs of complex conjugate zeros, such that between every two poles, there is a zero.

Theorem 1. Let $G(s) = \sum_{i=1}^N \frac{\alpha_i}{s^2 + \omega_i^2}$ such that $\alpha_i > 0$ for $i = 1, 2, 3, \dots$ and $\omega_1 < \omega_2 < \dots < \omega_N$. Then, between every two consecutive poles of $G(s)$ there exists a zero.

Proof. We begin with a truncated case of $G(s)$ denoted by $G_3(s)$ such that $G_3(s) = \sum_{i=1}^3 \frac{\alpha_i}{s^2 + \omega_i^2}$. Expanding, we get

$$G_3(s) = \frac{\alpha_1}{s^2 + \omega_1^2} + \frac{\alpha_2}{s^2 + \omega_2^2} + \frac{\alpha_3}{s^2 + \omega_3^2} = \{\alpha_1(s^2 + \omega_2^2)(s^2 + \omega_3^2) + \alpha_2(s^2 + \omega_1^2)(s^2 + \omega_3^2) + \alpha_3(s^2 + \omega_1^2)(s^2 + \omega_2^2)\} \{(s^2 + \omega_1^2)(s^2 + \omega_2^2)(s^2 + \omega_3^2)\}^{-1}.$$

The numerator of $G_3(s)$ is a polynomial in s^2 . Let this be known as $N(s^2)$. Then,

$$N(s^2) \big|_{s^2 = -\omega_1^2} = \alpha_1(-\omega_1^2 + \omega_2^2)(-\omega_1^2 + \omega_3^2) > 0$$

as $\alpha_i > 0 \quad \forall i$ and $\omega_1 < \omega_2 < \omega_3$. Similarly,

$$N(s^2) \big|_{s^2 = -\omega_2^2} = \alpha_1(-\omega_1^2 + \omega_2^2)(-\omega_1^2 + \omega_3^2) < 0$$

and

$$N(s^2) \big|_{s^2 = -\omega_3^2} = \alpha_1(-\omega_1^2 + \omega_2^2)(-\omega_1^2 + \omega_3^2) > 0.$$

$N(s^2)$ is a continuous function in s . The value of $N(s^2) \big|_{s^2 = -\omega_1^2}$ is positive, while at $N(s^2) \big|_{s^2 = -\omega_2^2}$ is negative. $N(s^2)$ must therefore be 0 for a value of s^2 somewhere between $-\omega_1^2$ and $-\omega_2^2$. Thus for $s^2 = -\omega_{z_1}^2$ such that $\omega_1 < \omega_{z_1} < \omega_2$, $N(-\omega_{z_1}^2) = 0$. Similarly, it can be shown that $N(-\omega_{z_2}^2) = 0$ where $\omega_2 < \omega_{z_2} < \omega_3$.

Using the same argument for the untruncated numerator of $G(s)$, it can be shown that there exist $n - 1$ zeros $\omega_{z_1}, \omega_{z_2}, \dots, \omega_{z_{n-1}}$ for $G(s) = \sum_{i=1}^N \frac{\alpha_i}{s^2 + \omega_i^2}$ such that, $\omega_1 < \omega_{z_1} < \omega_2 < \dots < \omega_{z_{n-1}} < \omega_N$, i.e. between every two consecutive poles there lies a zero. \square

The next theorem shows that for a system obtained by adding N second-order sections of the form $\frac{\alpha_i}{s^2 + \omega_i^2}$, the addition of a feed-through term $D \in \mathbb{R}$ can introduce a pair of complex conjugate zeros.

Theorem 2. Let $G(s) = \sum_{i=1}^N \frac{\alpha_i}{s^2 + \omega_i^2}$ such that $\alpha_i > 0 \quad \forall i$ and $\omega_1 < \omega_2 < \dots < \omega_N$. If $\tilde{G}(s) = G(s) + D$ where $D \in \mathbb{R}$ and $\tilde{G}(j\omega_z) = 0$ such that ω_z is not a zero of $G(s)$, then $\tilde{G}(s)$ can be written as $\tilde{G}(s) = (s^2 + \omega_z^2) \sum_{i=1}^N \frac{\beta_i}{s^2 + \omega_i^2}$.

Proof. At $s^2 = -\omega_z^2$, $\tilde{G}(s) = 0$. Substituting $s^2 = -\omega_z^2$ in $\tilde{G}(s)$, we have

$$\tilde{G}(j\omega_z) = \sum_{i=1}^N \frac{\alpha_i}{-\omega_z^2 + \omega_i^2} + D = 0.$$

Thus, $D = -\sum_{i=1}^N \frac{\alpha_i}{-\omega_z^2 + \omega_i^2}$.

Substituting the value of D in $\tilde{G}(s)$, we get

$$\begin{aligned} \tilde{G}(s) &= \sum_{i=1}^N \frac{\alpha_i}{s^2 + \omega_i^2} - \sum_{i=1}^N \frac{\alpha_i}{-\omega_z^2 + \omega_i^2} \\ &= \sum_{i=1}^N \alpha_i \left(\frac{1}{s^2 + \omega_i^2} - \frac{1}{\omega_i^2 - \omega_z^2} \right). \end{aligned}$$

Let $\frac{1}{\omega_i^2 - \omega_z^2} = k_i$. Then,

$$\begin{aligned} \tilde{G}(s) &= \sum_{i=1}^N \alpha_i \left(\frac{1 - k_i s^2 - k_i \omega_i^2}{s^2 + \omega_i^2} \right) \\ &= \sum_{i=1}^N -\alpha_i k_i \left(\frac{s^2 + \omega_i^2 - \frac{1}{k_i}}{s^2 + \omega_i^2} \right). \end{aligned}$$

Note that $\omega_i^2 - \frac{1}{k_i} = \omega_z^2$. Thus,

$$\tilde{G}(s) = \sum_{i=1}^N -\alpha_i k_i \left(\frac{s^2 + \omega_z^2}{s^2 + \omega_i^2} \right).$$

Let $-\alpha_i k_i = \beta_i$. Then $\tilde{G}(s) = (s^2 + \omega_z^2) \sum_{i=1}^N \frac{\beta_i}{s^2 + \omega_i^2}$. \square

A typical pole-zero plot of the collocated transfer function before and after addition of the feed-through term D is shown in figure 5. The pole locations remain the same even after adding the feed-through term.

For the cantilever beam used in the experiments, the collocated transfer function is:

$$\begin{aligned} G_{yu}(s) &= \frac{225}{s^2 + 0.3854s + 6035} + \frac{8971}{s^2 + 1.49s + 217100} \\ &+ \frac{90960}{s^2 + 3.573s + 1.697 \times 10^6} + 0.7456. \end{aligned}$$

This fixed structure form can be obtained approximately by using the *residue* function in MATLAB from the identified collocated model $G_{yu}(s)$ in figures 3 and 4. Due to the fully parameterized nature of the identified model, the residuals of

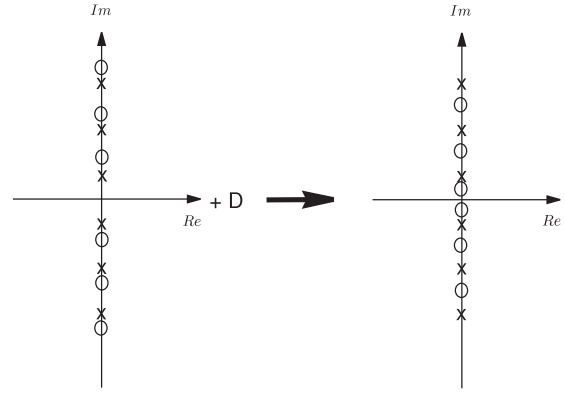


Figure 5. Poles (x) and zeros (o) of the collocated transfer function, before and after the addition of the feed-through term (D).

each second-order section will also contain a small ‘s’ term that can be neglected. Note that, in this case, $G_{yu}(s) \equiv \tilde{G}(s)$ (defined in theorem 2), where

$$\begin{aligned} G(s) &= \frac{225}{s^2 + 0.3854s + 6035} + \frac{8971}{s^2 + 1.49s + 217100} \\ &+ \frac{90960}{s^2 + 3.573s + 1.697 \times 10^6}, \end{aligned}$$

and

$$D = 0.7456.$$

The first resonant mode occurs at 12.33 Hz. Using theorem 2, it is found that a feed-through term of $D = -0.1372$ places a zero at 4.1858 Hz (arbitrarily chosen at a frequency less than the first resonant mode). Therefore, a feed-through term of $D_f = -0.8828$ was added to $G_{yu}(s)$.

As discussed in theorem 2, the addition of a low-frequency zero results in a phase inversion at dc relative to the original transfer function. The magnitude and phase response of the collocated open-loop and modified transfer functions, $G_{yu}(s)$ and $(G_{yu}(s) + D_f)$ respectively, are plotted in figure 7. A key observation is that the phase of the modified transfer function lies between 0° and -180° ; thus, a negative integral controller ($C(s) = \frac{-1}{s}$) in negative feedback, which adds a constant phase lead of 90° , will yield a loop transfer function whose phase response lies between $+90^\circ$ and -90° ; that is, the closed-loop system has a highly desirable phase margin of 90° . In the following two sections, two variations of an integral controller and a technique for gain selection are presented.

3.3. Integral resonant control design

The proposed integral resonant control, IRC, scheme is shown diagrammatically in figure 6. In the following, three suitable controllers—direct integral control and its two variants—are introduced and evaluated for performance and robustness. The frequency response of each controller is plotted in figure 8. Note that, in each case, the controller gain $\gamma > 0$ needs to be determined, as explained in section 3.4.

- *Simple integrator* $C(s) = \frac{-\gamma}{s}$: Integral control has been extensively researched and documented [17]. The main drawback in this application is the unnecessarily high sensitivity at low frequencies. A high control input at low frequencies may lead to actuator saturation.

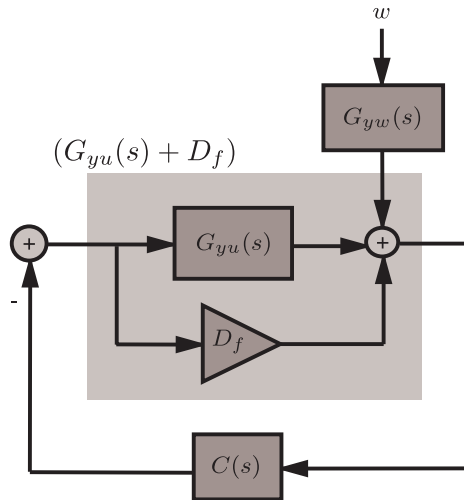


Figure 6. Schematic diagram of the implemented control strategy.

- *Lossy integrator* $C(s) = \frac{-\gamma}{s+p_1}$: This controller has reduced gain at low frequencies. To effectively reduce low-frequency gain, it is necessary to select p_1 close to the first structural resonance frequency. There is an associated penalty of slightly reduced closed-loop phase margin.
- *Band-pass filter* $C(s) = \frac{-\gamma s}{(s+p_1)(s+p_1)}$: To ensure the controller response rolls-off at low frequencies, a controller with two poles at $p_1 \text{ rad s}^{-1}$ and a zero at 0 rad s^{-1} is suitable. The resulting closed-loop phase margin is inferior to that exhibited by the two previous controllers, but the gain attenuation is greater. The situation can be improved by implementing $C(s) = \frac{-\gamma s}{(s+p_1)(s+p_2)}$, where $p_2 < p_1$.

3.4. Gain selection

Referring to the closed-loop schematic given in figure 6, the gain of the IRC can be determined by analysing the loop gain. A root-locus plot depicts the trajectories travelled by the poles with respect to an increase in the system gain, see figure 9. It is found that by increasing the controller gain, the poles follow a curve and finally reach the zeros with which they are paired. This plot also reveals the damping of each pole along the trajectory. As the gain increases, the poles initially move away from the imaginary axis and the damping increases until it reaches a maximum point. A further increase in gain drags the pole closer to the imaginary axis and reduces the damping. Finally, the pole is placed at the same position as its paired zero. At this position, the improvement in damping is negligible.

To achieve maximum damping of higher-frequency modes, higher gains are required. This high gain may place the low-frequency poles close to the imaginary axis (with no significant increase in damping) and thus low-frequency modes are not attenuated. In this work, as we are considering a cantilever beam with dominant low-frequency dynamics, a gain is chosen that provides optimal damping of the first three structural modes. For the system used in our experiments, the gain was found to be $\gamma = 550$.

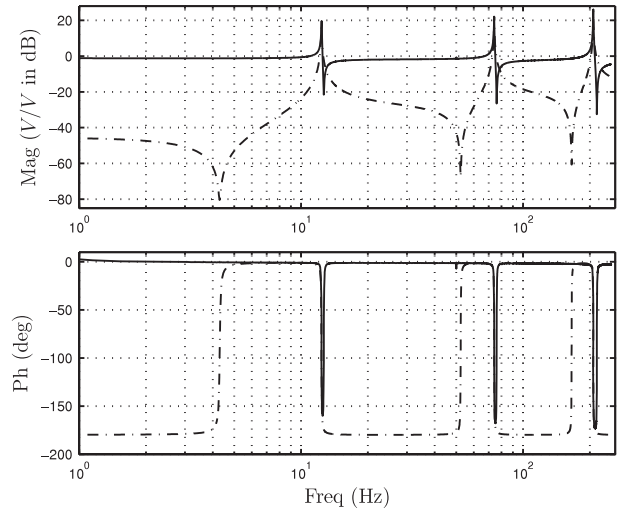


Figure 7. Open-loop collocated beam transfer function $G_{yu}(s)$ (—) and modified transfer function $(G_{yu}(s) + D_f)$ (- -).

3.5. Summary

The IRC controller design process can be summarized in the following steps:

- *Step 1:* Measure the open-loop frequency response of the system and preferably obtain a model for the system as described in section 3.1.
- *Step 2:* Use results in section 3.2. Determine the required feed-through term that adds a zero at a frequency lower than the first resonant mode of the system.
- *Step 3:* Design a controller of the form $C(s) = \frac{-\gamma s}{(s+p_1)(s+p_1)}$ by choosing p_1 to be approximately a decade lower in frequency than the first mode; see section 3.3.
- *Step 4:* By plotting the root-locus, select a suitable gain which results in peak attenuation at resonant frequencies lying in the band of interest; see section 3.4.
- *Step 5:* Implement IRC using either an analogue or digital transfer function. Measure the open- and closed-loop frequency responses and check that they agree with the simulated results, as shown in section 4.

4. Experimental results

The controller was implemented digitally using dSPACE with a sampling frequency of 20 kHz. The continuous transfer function of the controller is given by $C(s) = \frac{-550s}{(s+0.3(2\pi))(s+0.3(2\pi))}$. This was converted to a discrete transfer function using the zero-order hold approximation. To account for the system time delay, a time advance of one sample was incorporated into the control loop. This is achieved by multiplying the transfer function of the controller by the forward shift operator z . This is possible because $C(z)$ is strictly proper and has a relative degree of 1. Frequency responses are measured from the input disturbance w to the output tip displacement z of the cantilever beam, denoted by G_{zw} . Simulated open- and closed-loop frequency responses are shown in figure 10(a). Measured open- and closed-loop frequency responses are shown in figure 10(b). The first three modes are attenuated by 22, 24 and 21 dB, respectively.

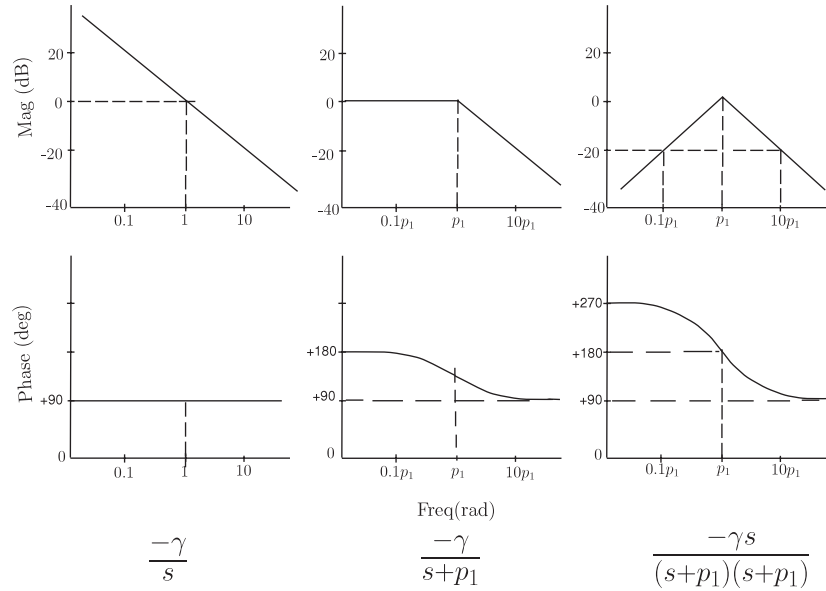


Figure 8. Typical bode plots of the three possible controllers assuming $\gamma = 1$.

Table 1. Damping for the first eight modes of the cantilever beam.

Mode number	1	2	3	4	5	6	7	8
Frequency (Hz)	12.33	74.25	207.48	408.75	682.32	1020.85	1427.23	1914.01
Attenuation (dB)	22	24	21	0.7	16	9	3	7

Table 2. Damping for the first eight modes for a cantilever beam with added mass.

Mode number	1	2	3	4	5	6	7	8
Frequency (Hz)	10.625	67.48	195.76	356.68	702.38	1028.98	1435.82	1921.97
Attenuation (dB)	17	19	20	0.5	4	4	1	5

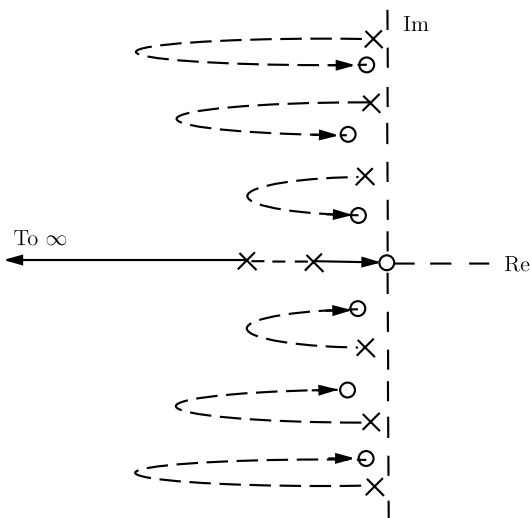


Figure 9. Root-locus plot showing the trajectories of the poles due to change in system gain.

To evaluate the controller performance at higher frequencies, frequency responses for the open- and closed-loop system are recorded for a larger bandwidth, from 0 to 2.5 kHz. This

band captures the first eight resonant modes of the cantilever beam. The open- and closed-loop responses depicting the first eight resonant modes are shown in figure 11.

Table 1 shows the attenuation achieved for the first eight modes. The minimal attenuation of the fourth mode is due to the position of the collocated patches.

To evaluate performance sensitivity to variations in resonance frequencies, open- and closed-loop responses were also taken after loading the cantilever beam with a mass. This is equivalent to adding uncertainty in the resonance frequencies. Even though the addition of mass shifts the resonant modes by as much as 10%, there is minimal performance degradation. All of the eight modes show significant damping, even with the mass present.

Figure 12 shows the open- and closed-loop responses of the cantilever beam with added mass. Table 2 documents the damping achieved on the loaded beam for the first eight modes.

5. Conclusions

This paper formalizes the pole-zero structure found in the transfer functions of collocated smart structures. It is shown that adding a feed-through term to the open-loop system introduces a new pair of resonant zeros. By adding a pair

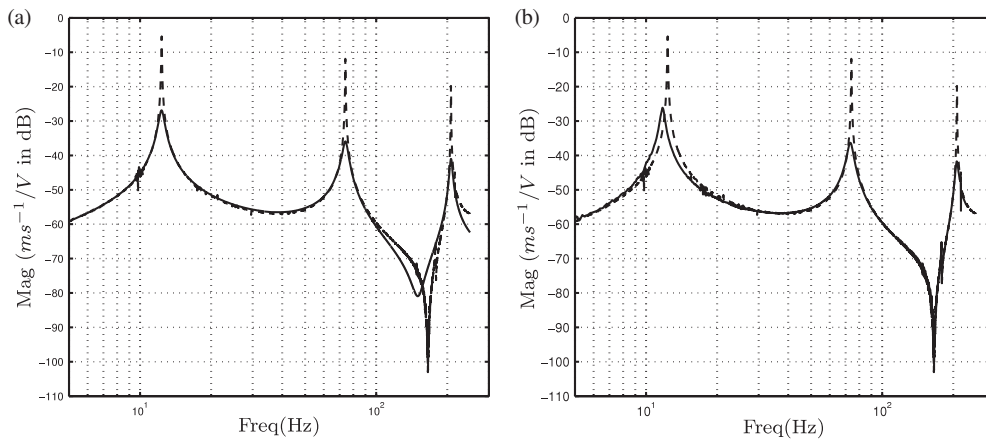


Figure 10. Simulated (a) and experimental (b) open-loop (---) and closed-loop (—) responses of the cantilever beam measured from disturbance input w to the tip displacement z .

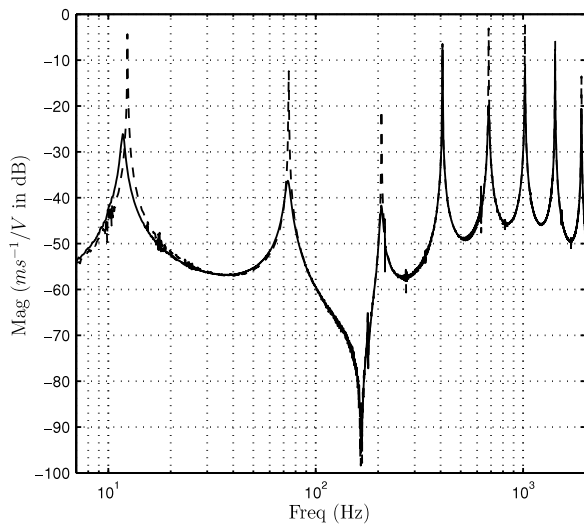


Figure 11. Open- (---) and closed-loop (—) system response for the first eight modes of the cantilever beam measured from disturbance input w to the tip displacement z .

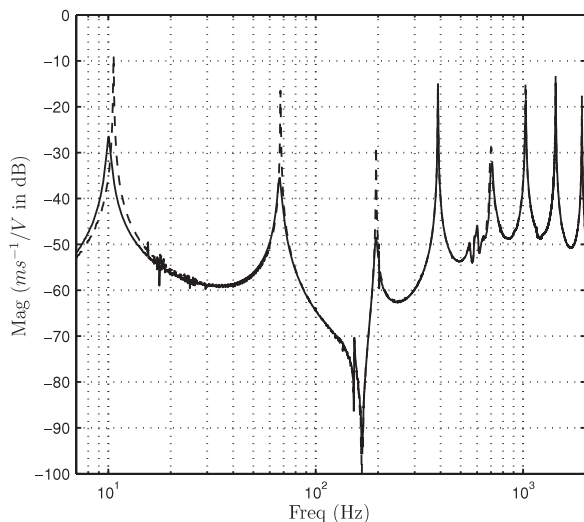


Figure 12. Open- (---) and closed-loop (—) system response for the additional mass-loaded cantilever beam measured from disturbance input w to the tip displacement z .

of zeros at a frequency below the first resonant mode, a simple first- or second-order controller is shown to provide good performance and stability margins. The so-called Integral Resonant Control scheme, IRC, is experimentally demonstrated to damp eight modes of a cantilever beam by up to 24 dB.

Acknowledgments

The authors would like to thank Dr Bharath Bhikkaji for his useful input.

This research was supported by the Australian Research Council and the ARC Center for Complex Dynamic Systems and Control.

References

- [1] Salapaka S, Sebastian A, Cleveland J P and Salapaka M V 2002 Design identification and control of a fast nanopositioning device *Proc. American Control Conf. (May 2002)* pp 1966–71
- [2] Vaillon L and Philippe C 1999 Passive and active microvibration control for very high pointing accuracy space systems *Smart Mater. Struct.* **8** 719–28
- [3] Wu S, Turner T L and Rizzi S A 2000 Piezoelectric shunt vibration damping of an F-15 panel under high-acoustic excitation *Smart Structures and Materials: Damping and Isolation, Proc. SPIE* **3989** 276–87
- [4] Crawley E F and de Luis J 1987 Use of piezoelectric actuators as elements of intelligent structures *AIAA J.* **25** 1373–85
- [5] Wang B T and Wang C C 1997 Feasibility analysis of using piezoceramic transducers for cantilever beam modal testing *Smart Mater. Struct.* **6** 106–16
- [6] Fuller C R, Elliott S J and Nelson P A 1996 *Active Control of Vibration* (New York: Academic)
- [7] Moheimani S O R and Fleming A J 2006 *Piezoelectric Transducers for Vibration Control and Damping* (Berlin: Springer)
- [8] Petersen I R and Pota H R 2003 Minimax LQG optimal control of a flexible beam *Control Eng. Practice* **11** 1273–87
- [9] Chen B M, Lee T H, Chang-Chieh H, Guo Y and Weerasooriya S 1999 An H_∞ almost disturbance decoupling robust controller design for a piezoelectric bimorph actuator with hysteresis *IEEE Trans. Control Syst. Technol.* **7** 160–74

- [10] Halim D and Moheimani S O R 2002 Experimental implementation of spatial H_∞ control on a piezoelectric laminate beam *IEEE/ASME Trans. Mechatron.* **4** 346–56
- [11] Halim D and Moheimani S O R 2002 Spatial H_2 control of a piezoelectric laminate beam: experimental implementation *IEEE Trans. Control Syst. Technol.* **10** 533–46
- [12] Fanson J L and Caughey T K 1990 Positive position feedback-control for large space structures *AIAA J.* **28** 717–24
- [13] de Silva C W 1999 *Vibration Fundamentals and Practice* (Boca Raton, FL: CRC Press)
- [14] Pota H R, Moheimani S O R and Smith M 2002 Resonant controllers for smart structures *Smart Mater. Struct.* **11** 1–8
- [15] McKelvey T, Akcay H and Ljung L 1996 Subspace based multivariable system identification from frequency response data *IEEE Trans. Autom. Control* **41** 960–78
- [16] Martin G D 1978 On the control of flexible mechanical systems *PhD Dissertation* Stanford University, USA
- [17] Preumont A 1997 *Vibration Control of Active Structures: An Introduction* (Dordrecht: Kluwer)
- [18] Hughes P C 1987 Space structure vibration modes: how many exist? which ones are important? *IEEE Control Syst. Mag.* **8** 22–8
- [19] Clark R L 1997 Accounting for out-of-bandwidth modes in the assumed modes approach: implications on collocated output feedback control *Trans. ASME J. Dynam. Syst. Meas. Control* **119** 390–5